Journal of Communications and Information Networks, Vol.2, No.1, Mar. 2017
DOI: 10.1007/s41650-017-0006-x

Research paper

Special Issue on Wireless Big Data

Analysis and prediction of 100 km-scale atmospheric duct interference in TD-LTE networks

Ting Zhou[1,3], Tianyu Sun[1,2,3], Honglin Hu[3*], Hui Xu[1,3], Yang Yang[1,3], Ilkka Harjula[4], Yevgeni Koucheryavy[5]

1. Key Lab of Wireless Sensor Network and Communication, Shanghai Institute of Microsystem and Information Technology, Chinese Academy of Sciences, Shanghai 201800, China
2. School of Information Science and Technology, ShanghaiTech University, Shanghai 201204, China
3. Shanghai Research Center for Wireless Communication, Shanghai 201204, China
4. VTT Technical Research Centre of Finland, VTT FI-02044, Finland
5. Tampere University of Technology, Korkeakoulunkatu 10, Tampere FI-33720, Finland

* Corresponding author, email: honglin.hu@mail.sari.ac.cn

Abstract: Atmospheric ducts are horizontal layers that occur under certain weather conditions in the lower atmosphere. Radio signals guided in atmospheric ducts tend to experience less attenuation and spread much farther, i.e, hundreds of kilometers. In a large-scale deployed TD-LTE (Time Division Long Term Evolution) network, atmospheric ducts cause faraway downlink wireless signals to propagate beyond the designed protection distance and interfere with local uplink signals, thus resulting in a large outage probability. In this paper, we analyze the characteristics of ADI atmospheric duct interference (Atmospheric Duct Interference) by the use of real network-side big data from the current operated TD-LTE network owned by China Mobile. The analysis results yield the time varying and directional characteristics of ADI. In addition, we proposed an SVM (Support Vector Machine)-classifier based spacial prediction method of ADI by machine learning over combination of real network-side big data and real meteorological data. Furthermore, an implementation of ADMM (Alternating Direction Methods of Multipliers) framework is proposed to implement a distributed SVM prediction scheme, which reduces data exchange among different regions/cities, maintains similar prediction accuracy and is thus of a more practical use to operators.

Keywords: TD-LTE, interference map, atmospheric duct, machine learning, wireless big data

Citation: T. Zhou, T. Y. Sun, H. L. Hu, et al. Analysis and prediction of 100 km-scale atmospheric duct interference in TD-LTE networks [J]. Journal of communications and information networks, 2017, 2(1): 66-80.

1 Introduction

LTE (Long-Term Evolution) is a standard for the high-speed wireless communication for mobile phones and data terminals. According to the recent study by 5G Americas (http://www.4gamericas.org/en/newsroom/press-releases/north-america-hits-60-lte-market-share), LTE technology has owned 60% of market share in North America, and 34% in Oceania and Asia. The number of global LTE users has reached 1.29 billion. LTE supports both the TDD (Time Division Duplex) and FDD (Frequency Division Duplex) modes. By the end of July 2016, the users' number of TD-LTE (also known as LTE-

Manuscript received Dec. 26, 2016; accepted Feb. 8, 2017
This research is partially funded by the National Natural Science Foundation of China (Nos. 61461136004, 61631013), Ministry of Science and Technology International Cooperation Project (No. 2014DFE10160) and Shanghai Municipality of Science and Technology Commission Project (Nos. 17QA1403800, 17ZR1429000).

TDD) reached 430 million and maintained a high growth speed (https://www.chinatechnews.com/2016/07/25/23806-china-mobile-now-counts-430-million-4g-users).

Furthermore, because TD-LTE uses a single frequency band for both uplink and downlink transmissions, downlink signals from other BSs (Base Stations) may cause CCI (Co-channel Interference) on the uplink signals of local BSs, which is denoted by downlink-to-uplink interference. To prevent the downlink-to-uplink interference, TD-LTE networks are accurately synchronized and a GP (Guard Period) is set in the special sub-frame of the TDD frame structure. The special sub-frame has a duration of 1 ms (14 OFDM symbols) and consists of three parts: DwPTS (Downlink Pilot Time Slot), GP and UpPTS (Uplink Pilot Time Slot). In GP, the system does not transmit any information to prevent the CCI from the downlink signals of adjacent BSs to local cell's uplink signals. Depending on the business requirements, there are nine configurations of special sub-frame in TD-LTE systems. Typically, operators only configure 2 OFDM symbols for GP, in order to improve the transmission efficiency. The corresponding protection distance is 42 km. When GP is configured with 10 OFDM symbols at most, sacrificing a large part of transmission efficiency, the protection distance increases by 5 times.

An atmospheric duct is a horizontal layer in the lower atmosphere in which the vertical refractive index gradients are such that radio signals (and light rays) are guided, and tend to propagate within the duct boundaries. Moreover, they experience less attenuation in the ducts than they would if the ducts were not present. In 1968, Bean and Dutton[1] firstly set up the formula of atmosphere refractivity and proposed the presence criterion of atmospheric ducts.

Ref. [2] indicates that the ducting could lead to a variety of effects, such as the loss of propagation, altitude errors for height-finding radars, decreased/increased detection ranges and shortened/extended radio horizons. In radar system, evaporation ducting can reduce detection ranges[3]. Surface-based ducts give rise to effects including clutter rings in the radar's plan position indicator, height errors for 3-D radar, and contamination of automated rain-rate calculations from weather radars[4]. In Ref. [5] Oraizi and Hosseinzadeh studied the effects of atmospheric duct on OFDM-Based digital broadcasting systems. The study reveals that the ducts amplify the strength of EM (Electromagnetic) signal thereby causes interference effects on adjacent services and reduces the frequency reuse distance.

As a result of the atmospheric duct effect, in TD-LTE networks, downlink signals from a faraway BS beyond the protection distance of the GP may interfere with the uplink signals of a local BS, which is denoted by ADI (Atmospheric Duct Interference). Moreover, ADI severely impacts the performance of TD-LTE networks. From the real network-side data provided by China Mobile, one day when ADI occurred in Xuzhou, Jiangsu Province, about 27.6% of cells experienced uplink interference higher than -90 dBm, which may totally submerge the useful signal and block the total communication of the cell. Therefore, ADI issues are in pressing need to be analyzed and solved.

There are two main methods to detect and estimate atmospheric ducts: (1) using radiosonde measuring temperature, pressure and humidity with height and computing the atmospheric modified refractivity[2]; and (2) using radar sea clutter to forecast the ocean refractive section plane[6]. Method (1) poses the problems of a high measuring difficulty, high cost and military secrecy issue, whereas method (2) is usually used in ocean scenarios, and is not suitable for land scenarios. Moreover, these methods are only focused on atmospheric ducts, but also the answers to some key questions of ADI, such as; what are the characteristics of ADI? When will ADI occur How does one identify and estimate ADI? The answers to these questions are still unknown and require in-depth analyses. Other than interference analysis, the prediction of ADI is also an essential problem to operators, to avoid the impact of ADI and improve the network performance.

In this paper, we innovatively use the real network-side big data from China Mobile to per-

form interference analysis. We visualize the interference data using map-based methods, and obtain the characteristics of ADI on time and space in large-scale TDD networks. We combine the network side big data and the meteorological data to perform the ADI prediction. Taking the novelty of the problem and the huge amount of data into consideration, we employ a famous machine learning algorithm-SVM (Support Vector Machines) to predict ADI. Moreover, because the SVM algorithm is a centralized machine learning method, it is inefficient due to a large amount of data gathering and exchanging. We therefore further proposed an implementation of the ADMM (Alternating Direction Methods of Multipliers) framework, to perform a distributed SVM prediction scheme. Our work fills the gap in the ADI research of large-scale TDD mode communication, and helps mobile operators improve the interference coordination and network optimization performance, under atmospheric duct scenarios.

The rest of this paper is organized as follows. In section 2, we illustrate the impacts of ADI on TD-LTE networks. We propose a map-based interference visualization method in section 3. The characteristics of ADI are analyzed based on the real network-side big data in section 4. We propose an SVM-classifier based spacial prediction method of ADI in section 5. In section 6, a distributed SVM algorithm based on the ADMM framework is proposed to implement ADI spacial prediction in practical networks. Finally, we present the conclusions of this paper in section 7.

2 Overview of ADI

2.1 The system design of TD-LTE to prevent downlink-to-uplink interference

TD-LTE works in time division duplex mode. Base stations and users use the same frequency band. Different time slots are employed to distinguish between uplink and downlink. In TD-LTE, there exists three kinds of subframes: uplink, downlink and special sub-frame. Special sub-frame consists of three parts: DwPTS (Downlink Pilot Time Slot), GP (Guard Period), UpPTS (Uplink Pilot Time Slot). Moreover, the GP is located at the moment when downlink convert to uplink to prevent the interference from downlink signals to uplink signals. Fig. 1(a) shows the frame structure of TDD system. The downlink signal from an adjacent BS arrives at the GP, so it would not interfere with local uplink signals.

To satisfy different requirements, TD-LTE supports multiple kinds of special sub-frame configurations. As Tab. 1 shows. Configuration 7 is the normal setting of TD-LTE network and has 2 OFDM symbols for GP. Therefore the protection distance for preventing downlink-to-uplink interference is $C \times T_{\mathrm{sf}} \times \frac{2}{14}$, where C is the speed of light and T_{sf} is the length of sub-frame, which is equal to 1 ms. The protection distance is then calculated as 42 km. Configuration 0 has the largest GP of 10 OFDM symbols and its protect distance is 214 km. Under normal circumstances, any downlink signals from distant BSs beyond the maximum protection distance would experience enough attenuation and hardly interfere with the local uplink signals.

2.2 The atmospheric ducts phenomena

Anomalous propagation conditions in the atmosphere result from variations in the refractivity of the atmosphere[2]. The refractivity is given by

$$N = \frac{77.6}{T}\left(p + \frac{4810e}{T}\right). \tag{1}$$

Here, N is the dimensionless refractivity (N-units), T is the absolute temperature in K, p is the barometric pressure in hPa, and e is the water vapor pressure in hPa. To consider the effect of the earth's curvature, a modified refractivity M is given as

$$M = N + \frac{z}{R_{\mathrm{e}} \times 10^{-6}}, \tag{2}$$

where M is the dimensionless modified refractivity (M-units), z is the height above the earth's surface, and R_{e} is the earth's radius. In the normal atmosphere, M increases with altitude. An atmospheric

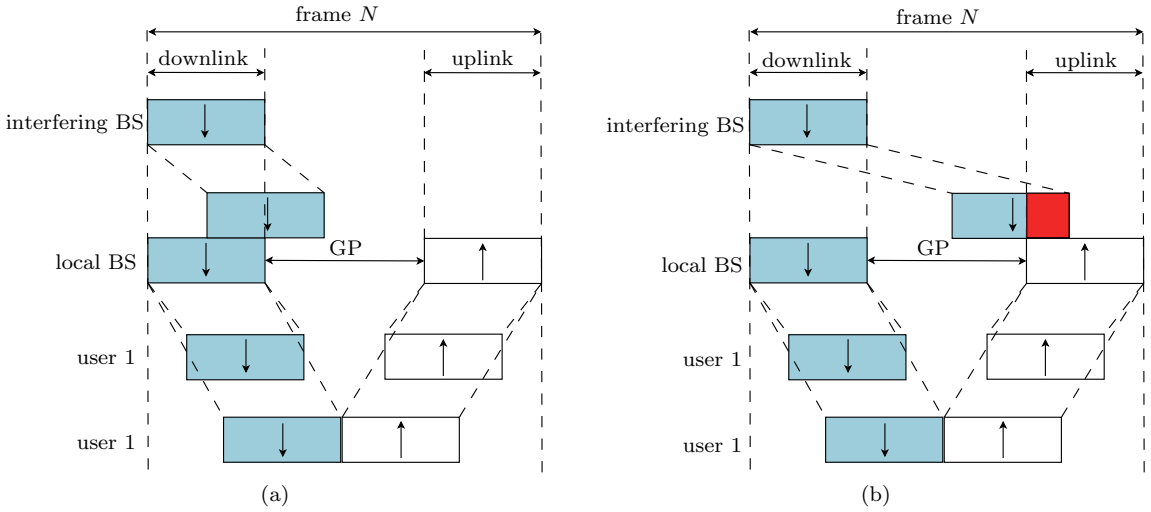

Figure 1 Frame structure of TDD system. (a) Without ADI; (b) with ADI

Table 1 Configuration table of special sub-frame (unit: OFDM symbol)[7]

configuration ID	conventional cyclic prefix			extended cyclic prefix		
	DwPTS	GP	UpPTS	DwPTS	GP	UpPTS
0	3	10	1	3	8	1
1	9	4		8	3	
2	10	3		9	2	
3	11	2		10	1	
4	12	1		3	7	2
5	3	9	2	8	2	
6	8	3		9	1	
7	10	2				
8	11	1				

duct occurs for all negative M gradients. Signals will be trapped in the height of negative M gradients.

Fig. 2(a) shows the modified refractivity M with altitude of surface ducts, surface-based ducts and elevated ducts respectively. The area of negative M gradient is the ducting layer. Fig. 2(b) shows the real refractivity M measured by radiosonde in Baoshan, Shanghai, China. It can clearly ne observed that between the heights of 250 m and 320 m there exists the ducting layer. Radio signals (and light rays) are guided or ducted in the ducting layer, tend to propagate within the duct boundaries, thus experiencing less attenuation in the ducts than they would if the ducts were not present.

2.3 Impact of ADI on TD-LTE networks

Under abnormal conditions, signals would propagate in the ducting layers with little attenuation. As a result, downlink signals from other BSs beyond the maximum protection distance of GP may still cause CCI (Co-Channel Interference) on local BSs' uplink signals. This is denoted by atmospheric duct interference, i.e. ADI. In the existing literatures, CCI has been widely studied for a long while. According to 3GPP, TD-LTE networks apply ICIC (Inter Cell Interference Cancellation Coordination) technology to solve co-channel interference problem. Basically, BSs generate information of interference of RB (Re-

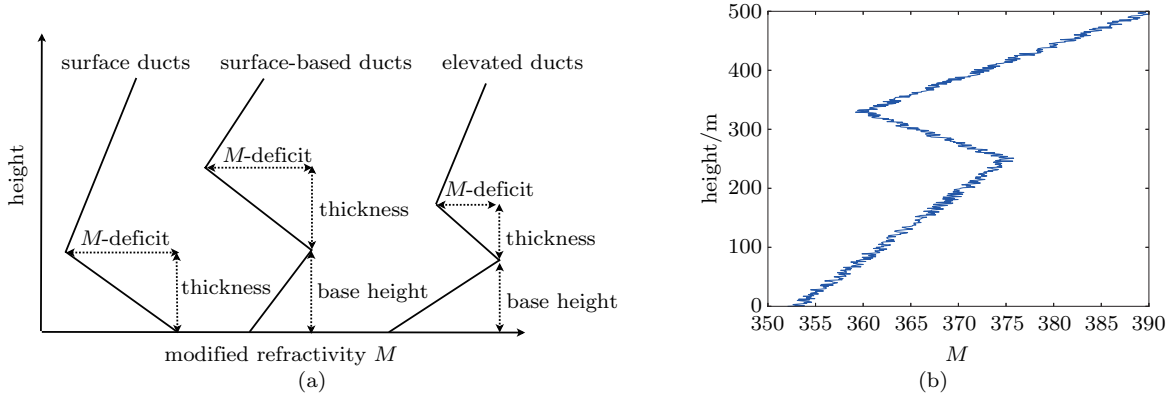

Figure 2 Illustration of anomalous atmospheric conditions based on modified refractivity M with altitude. (a) M with altitude of different ducts; (b) the real M measured by radiosonde in Baoshan

source Block) and pass the information to adjacent BSs through X2 interface to make resource allocation decisions[8]. Ref. [9] gives an overview of the research on the CCI. A power control based time-domain ICIC scheme is proposed in Ref. [10]. Moreover, Ref. [11] proposes a method of channel estimation by estimating the interference covariance parameters. A method is presented to cancel CCI at the mobile user side based on a realistic cell-edge scenario in WiMAX system[12]. Ref. [13] proposes a CCI cancellation strategy based on SIC (Successive Interference Cancellation) for communication systems. However, the current study mentioned above mainly focus on the user-side downlink CCI. They are based on the accurate channel estimation or the cooperation of adjacent BSs. The localization techniques widely used in wireless sensor network[14] is not suitable either. This is because the TDD system can not separate signals from remote BSs from signals from local users. Thus we can not localize interference sources via wireless received signal strengths.

Recall that we derived the maximum protection distance of the TD-LTE system as 214.3 km. Theoretically, if the synchronization of the system is perfect, any BSs in this range will not interfere the uplink signals of local BS. Under normal circumstances, the downlink signals from farther BSs would attenuate to a negligible level. However, network-side data from China Mobile shows that large-scale downlink-to-uplink interference sometimes arises severely and affects the network service of a large region. Moreover, the current ICIC or network optimization methods are of no use. This is because in the scenario when the atmospheric duct effect is present, the downlink signals from other BSs that are far beyond the maximum protection distance of GP may experience very little attenuation and interfere with the uplink signals of the serving BS. This is shown in Fig. 1(b). As a result, the CCI caused by the atmospheric duct, i.e. ADI, has a large impact on the large-scale deployed TD-LTE networks. Figs. 3 and 4 show the real interference situation of the commercial operated TD-LTE networks by China Mobile in the Jiangsu Province, on May 16, 2016.

Analysis of ADI is worth studied. Current difficulties are 1) the difficulty in identifying the source of interference, due to the interference that may come from a very remote BS; 2) the interfered regions are very large, usually covering several cities, and the distance of the interferences propagate on a large scale (200 km or even farther); 3) the occurrence time of ADI is difficult to predict. These characteristics make the conventional interference analysis and management methods unsuitable for use.

3 Map-based 100 km-scale ADI analysis method

In order to analyze the characteristics of a 100 km-scale ADI, we obtain from China Mobile the real

network-side interference data of the all the base stations of Jiangsu province, for the day when ADI occurs.

3.1 Map-based visualization of 100 km-scale interference data.

To begin our analysis, the first step is to visualize the interference data. This will provide us with the most intuitive feeling on the general interference conditions. An interference map is a useful tool. The interference map defines the RF (Radio Frequency) power distribution in the time and space. In our paper, the RF signal power can be measured at the position of every antenna of BSs to create a map over the whole Jiangsu province. The space domain includes information of the latitudes and longitudes of the BSs, the antenna heights and the angles of sectors for each antenna.

In total, there are more than fifty thousand measuring points in Jiangsu province. They are disorderly distributed. Therefore, we firstly rasterize the interference level in the space domain, to convert the data to a $M \times N$ matrix X.

Set all elements of X 0. Let lo_i, la_i, le_i represent the longitude, latitude and interference level of ith measuring point, respectively. Moreover, let $lo_{\min}$, $lo_{\max}$, $la_{\min}$, $la_{\max}$ represent respectively the minimum and maximum values of the longitude and latitude of Jiangsu province, respectively. Let $le_{\min}$, $le_{\max}$ represent the minimum and maximum values of the interference level. And let $lo_{\text{step}} = \dfrac{lo_{\max} - lo_{\min}}{M}$, $la_{\text{step}} = \dfrac{la_{\max} - la_{\min}}{N}$,

$$\begin{aligned} X_{m,n} &= \frac{1}{K}\sum_{i=1}^{K} le_i \cdot I_{A,\ B}(lo_i, la_i), \\ m &= 0, 1, 2, \cdots, M-1, \\ n &= 0, 1, 2, \cdots, N-1, \end{aligned} \tag{3}$$

where A is interval $[lo_{\min} + mlo_{\text{step}}, lo_{\min} + (m+1) \times lo_{\text{step}})$ and B is interval $[la_{\min} + mla_{\text{step}}, la_{\min} + (m+1)la_{\text{step}})$, $I_{A,\ B}(x, y)$ is the indicator function

$$I_{A,\ B}(x, y) = \begin{cases} 1, & \text{if } x \in A \text{ and } y \in B, \\ 0, & \text{otherwise.} \end{cases} \tag{4}$$

Now, the space information and interference information has been merged into the same matrix. The next step is to use interpolation to increase the resolution of the data. Because of the positions of actual BSs, after the rasterizing, some elements of matrix X may have no data. In this case, spatial interpolation techniques can be utilized to estimate values of these points that have not been measured. The spatial interpolation techniques are traditionally used in the context of GIS (Geographic Information Systems)[15]. We employ the Kriging interpolation[16] which is expressed briefly as follows.

Kriging interpolation uses a weighted sum of all known data points on the space to estimate the unknown point.

$$\hat{z}_0 = \sum_{i=1}^{n} \lambda_i z_i. \tag{5}$$

$\hat{z}_0$ is the estimation of point (x_0, y_0), $z_0 = z(x_0, y_0)$. λ_i is the weights. It is calculated by the following optimization problem

$$\begin{aligned} \min_{\lambda_i} \quad & Var(\hat{z}_0 - z_0) \\ \text{s.t.} \quad & E(\hat{z}_0 - z_0) = 0. \end{aligned} \tag{6}$$

After performing rasterizing and interpolation, we can create the interference map of the region concerned, i.e. Jiangsu province. We summarize the complete procedure of the map-based visualization of interference data as follows.

Algorithm 1 Process of map-based visualization of interference data

1 Input the set of longitude, latitude and interference level for each BS, lo, la, le;

2 Determining M and N. Usually $M \times N$ is approximately $\frac{1}{10}$ of the total number of BSs approximately. $X_{m,n} = \frac{1}{K}\sum_{i=1}^{K} le_i \cdot I_{A,\ B}(lo_i, la_i)$. Generate X;

3 For $x_{i,j}$ in X, if $x_{i,j} = 0$ and (i, j) in the province range, use the nearest 30 points of (i, j) doing kriging interpolation to get $\hat{x}_{i,j}$;

4 For $x_{i,j}$ in X, if $x_{i,j} = 0$ and (i, j) out of the province range, $x_{i,j} = \lfloor le_{\min} \rfloor$;

5 Render X using the heatmap;

6 Return interference map.

3.2 Correlation analysis of the interference map

In a TD-LTE system, because uplink and downlink use the same frequency band and the channel reciprocity is confirmed, we can naturally infer that ADI has the property of reciprocity, which means if BS A brings ADI to BS B, then BS B would also interfere with BS A. Therefore, in order to address the issue of identifying the potential interfered areas and the interference source of ADI, we try to look for the correlation of the interference data within the whole Jiangsu province.

We employ the Pearson correlation coefficient to obtain the one pair of interference objects. Firstly, we divide the interference map into a plurality of square regions. Then we compute the mean values of interference levels larger than a threshold in each square region, at different time periods. Setting the threshold is performed to eliminate the influence of interference-free areas.

As a result, each region has an interference vector, in which each element represents the mean interference level at a certain measuring time. The correlation coefficients between the interference vectors of the regions of any pair can then be computed. If the correlation coefficient is closer to 1, the possibility of existing atmospheric ducts between the corresponding two regions is higher. In other words, we can find certain possible pairs of interference objects.

In order to further verify our conjecture, we employ the sector angle data of all antennas of the BSs in the Jiangsu province to analyze the directional characteristic of ADI. Similar to the map-based visualization method of interference data, we first divide the interference map into a plurality of square regions. Thereafter, we set a global threshold and record the information of the sector angles in each region, for all antennas with interferences larger than the threshold. Typically, the sector angles of each BS are around 0°, 120° and 240°. If the distribution of sector angles filtered by the threshold focus on a certain degree, it indicates that the interference is directional and that we can use it to find the source direction of interference. By the combination of the results of correlation coefficients and sector angle analysis, the ADI pair of regions can be identified.

4 Analysis of 100 km-scale ADI

We use the network-side data of Jiangsu province, from China Mobile, to analyze the ADI characteristics. The analysis settings are as follows. The data is collected from 244 375 antennas in Jiangsu, including the longitudes, latitudes, antenna heights, sector angles and interference levels. When rasterizing, we make $M = 160$ and $N = 160$. When performing Kriging interpolation to decrease the computational complexity, we only use the nearest 30 points to the target point.

According to the network-side data at different times on May 16, 2016, provided by China Mobile, Fig. 3 (a)∼(d) are the interference maps at 1:00 am, 7:00 am, 13:00 pm and 19:00 pm, respectively. After interpolation, the whole map appears natural, continuous and smooth. In Fig. 3(a), the interference level was rising, and reached the highest level in Fig. 3(b). Thereafter, the interference level fell, and in Fig. 3 (c) and (d), the interference level and distribution were normally steady and under the network tolerance threshold. That means that from 1:00 am∼7:00 am on May 16, 2016, ADI may have probably occurred. From the explanation of meteorology, usually from the midnight to the morning, the temperature of ground drops quickly and the lower atmosphere prone to temperature inversion. That means that in a certain height range, the atmosphere temperature rises in pace with the increasing height. According to Eq. (1), the refractivity M has negative gradients and thus causes the atmospheric duct phenomenon.

In addition, in the middle and northern regions in Fig. 3(b), the average interference level can reach up to −90 dBm, whereas a good quality of service usually requires that of less than −100 dBm. With respect to the geographical situation of Jiangsu province, we find that these severely interfered ar-

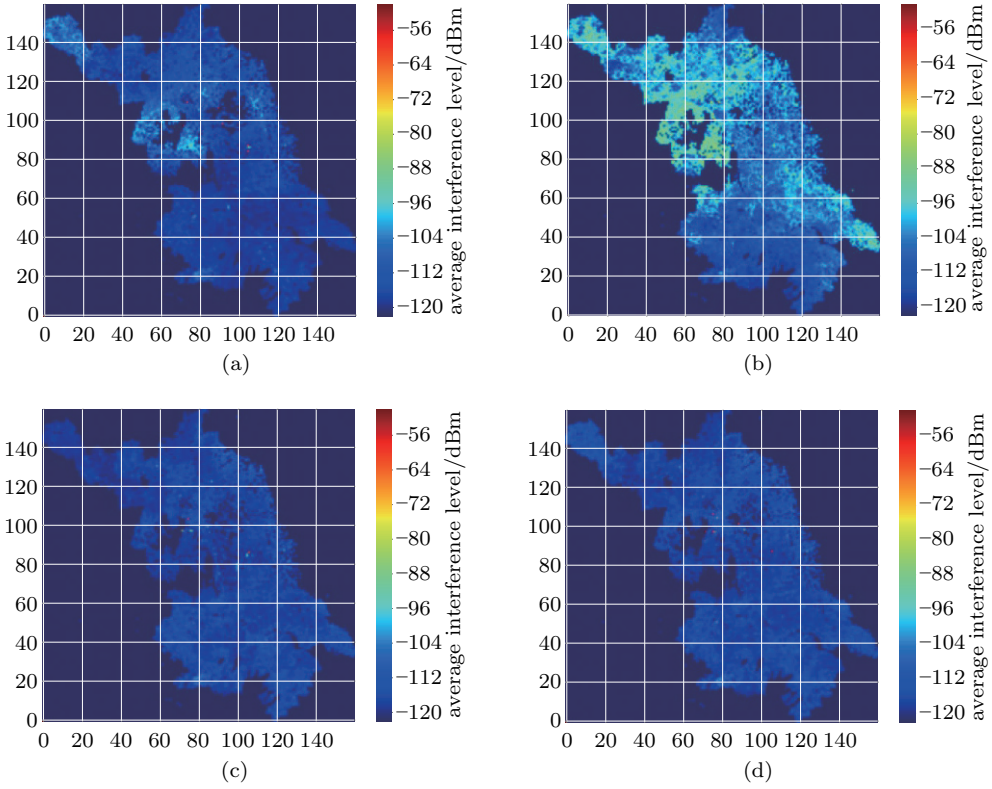

Figure 3 Illustration of the property of reciprocity in atmosphere duct interference. (a) 1:00; (b) 7:00; (c) 13:00; (d) 19:00

eas are mostly rural regions. It can be understood that in the rural regions the space is very open, and this is suitable for the propagation of electromagnetic waves. However, in the city, a large number of high-rise buildings would hinder the spread of the interference signals, thus the interference level is reduced.

As a result: (1) ADI has a time varying characteristic and probably occurs from the midnight to the morning; and (2) ADI has the feature of territoriality, and the rural regions have a higher probability to suffer from ADI.

Fig. 4 shows the interference map at 2 am. We can easily find the severe ADI regions marked by red circle, which are denoted by area1, area2 and area3, respectively. Compared with the situation at 1:00am, the interference levels of the three areas clearly increase simultaneously. According to the map scale, the distances from area1 to area2/area3 are larger than the maximum protection distance of TD-LTE networks, thus there exists ADI between them. The ADI pairs of area1-area2 and area1-area3 verify our guess of the ADI reciprocity property.

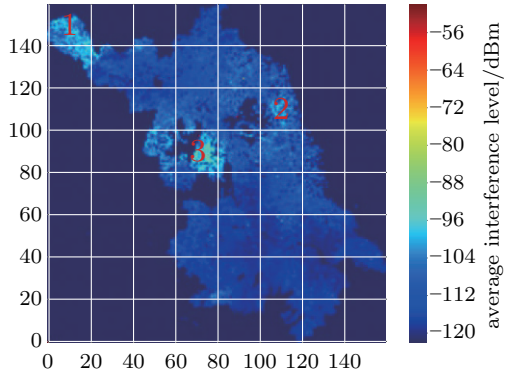

Figure 4 Illustration of reciprocity property of atmosphere duct interference

Furthermore, we divide the interference map into an 8×8 grid, and extract interference data every 1 h from 0:00 am∼7:00 am, when the interference phenomenon exists, in order to calculate the correlation coefficients between each of the areas. We set

the interference convex of area1 as the benchmark. Fig. 5 shows the correlation coefficients on the map. It can be seen that in the adjacent regions of area1, the correlation coefficient is low. Apparently, these regions are in the range of GP's protection distance. Therefore, they will not be interfered with, even if the atmospheric ducts exist. The regions with correlation coefficients that are bigger than 0.9 are in the middle eastern part of Jiangsu, in which area2 and area3 are located. The result coincides with that shown in Fig. 5.

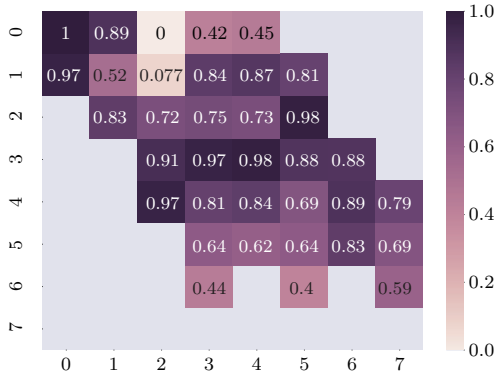

Figure 5 Correlation coefficients between each region

Fig. 6 gives the distribution of sector angles of the ADI pair: area1-area2. The reference direction is north, and the rotation is clockwise. Fig. 6 (b) and (c) show the distribution of the sector angles of the BSs in area2 and area3, which have interference levels that are larger than −100 dBm. It is clear that the direction of 240° suffers much from ADI, which is just the direction toward area1. Fig. 6(a) shows the distribution of sector angles of BSs in area1, with interference levels that are larger than −100 dBm. The distribution focus is on 120° and 240°, where 120° is toward area2 and area3. The interference from 240° of area1 may probably come from the provinces adjacent to Jiangsu, such as the Henan province and Anhui province. The result from Fig. 6 also coincides with that from Figs. 4 and 5, thus further verifying the directional characteristic and reciprocity property of ADI.

Therefore, we have: (3) ADI has a directional characteristic and the property of reciprocity. (4) If the correlation coefficient of the interference data in two regions is closer to 1, the corresponding two regions have a high probability to be pair of ADI objects.

5 An SVM-classifier-based spacial prediction method

5.1 Problem formulation

Support vector machine is a machine-learning algorithm. It is considered to be one of the best classification algorithms. Classification means that if we have some sets of things classified; when new data arrives, SVM can predict which set it should belong to. In our problem, the inputs are the information of the BSs and weather conditions. The output is 1 or −1, which indicates whether or not the BSs will be affected by ADI, respectively. In the binary class, SVM classifiers often have superior accuracy rates and considerable generation abilities. Moreover, the SVM-classifier can find a robust hyperplane to split the positive and negative samples.

Given a set of positive and negative samples, the goal of SVM is to find a hyperplane to split the positive and negative samples. However, it does not just easily split them; the principle is to make the margin between the positive and negative samples maximum. The hyperplane can be described by $\boldsymbol{\omega}^{\mathrm{T}}\boldsymbol{x}+b=0$. The hyperplane is decided by normal vector $\boldsymbol{\omega}$ and intercept $\boldsymbol{b}$. Assume we have training sample collection $D=\{(\boldsymbol{x}_1,y_1),(\boldsymbol{x}_2,y_2),\cdots,(\boldsymbol{x}_N,y_N)\}$. $y_i \in \{+1,-1\}$ is the label of samples. We use this samples training to get a linear classfier (hyperplane): $f(\boldsymbol{x})=\mathrm{sign}(\boldsymbol{w}^{\mathrm{T}}\boldsymbol{x}+b)$. As Fig. 7 shows, the margin is $\dfrac{2}{\|\boldsymbol{\omega}\|}$. And both positive and negative points satisfy that $y_i(\boldsymbol{\omega}^{\mathrm{T}}\boldsymbol{x}_i+b)\geqslant 1$.

In our application, we use this classifier to predict whether the BSs in the test set will be interfered by ADI or not after learning the training sets of BSs. The $\boldsymbol{x}_i$ includes the network-side information of BSs and meteorological information. Specifically, it consists of latitude and longitude of BS, time, sector

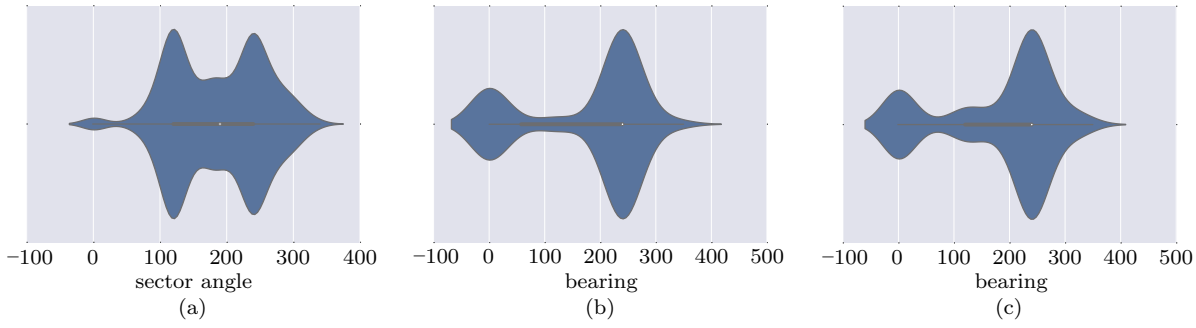

Figure 6 The distribution of sector angles. (a) area1; (b) area2; (c) area3

angles, antenna height and meteorological data.

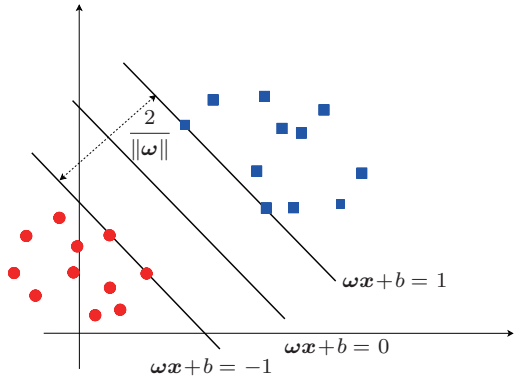

Figure 7 Support vector machine and margin

Maximizing the margin $\frac{2}{\|\boldsymbol{\omega}\|}$ is equal to minimizing $\frac{1}{2}\|\boldsymbol{\omega}\|^2$. However, in practice, it is difficult to get a hyperplane that can compeletely separate the different classes of samples. To make the classifier more robust, we introduce soft margin to allow some points not to satisfy the constraint: $y_i(\boldsymbol{\omega}^{\mathrm{T}}\boldsymbol{x}_i+b) \geqslant 1$. Obviously, when we maximize the margin, we should keep the samples that don't satisfy the constraints as few as possible.So the optimaztion problem can be written as

$$\min_{\boldsymbol{w},b} \frac{1}{2}\|\boldsymbol{\omega}\|^2 + C\sum_{i=1}^{m}\max(1-y_i(\boldsymbol{\omega}^{\mathrm{T}}\boldsymbol{x}_i+b),0)^2, \quad (7)$$

where C is constant and $\max(1-y_i(\boldsymbol{\omega}^{\mathrm{T}}\boldsymbol{x}_i+b),0)^2$ is the square of hinge loss function $l_{\mathrm{hinge}}(z) = \max(0,1-z)$. We use it to avoid overfitting and linearly indivisible condition. By introducing slack variables $\xi_i \geqslant 0$, Eq. (7) can be rewritten as

$$\min_{\boldsymbol{\omega},b,\boldsymbol{\xi_i}} \frac{1}{2}\|\boldsymbol{\omega}\|^2 + C\sum_{i=1}^{m}\xi_i.$$
$$\text{s.t.} \begin{cases} y_i(\boldsymbol{\omega}^{\mathrm{T}}\boldsymbol{x}_i+b) \geqslant 1-\xi_i \\ \xi_i \geqslant 0, \ i=1,\cdots,m. \end{cases} \quad (8)$$

This is a quadratic programming problem. We can use the common quadratic programming algorithm to solve it. Furthermore, in Ref. [17], a novel algorithm named SMO (Sequential Minimal Optimization), which can avoid the complicated inverse of the Hessian matrix in each iteration.

5.2 The prediction result of SVM

Our training data comes from two aspects: 1) the network-side data containing the longitude, latitude, time, sector angles, and interference indicator (threshold of −100 dBm); and 2) meteorological data from the China meteorological data website containing air temperature, air pressure and vapor pressure, i.e. the three key physical factors in formula (1). In this case, each sample consists of ($\boldsymbol{x}_i$, y_i) representing the data of a BS, where y_i is the interference indicator which determines whether or not the BS is affected by ADI under the interference threshold of −100 dBm; and is a vector consisting of the rest of the components, i.e., the longitude, latitude, time, sector angles, air temperature, air pressure, vapor pressure, etc.

The simulation is carried out under the cases wherein the number of training sets are 2 000, 4 000,

10 000, 20 000 and 40 000. After training, the classifier is used to predict the interference indicator of a testing set having a size that is 20% of the training sets. A well-known KNN (K Nearest Neighbor)[18] algorithm is used as our benchmark. In KNN an object is classified by a majority vote of its neighbors, with the object being assigned to the class most common among its k nearest neighbors. Here we make $k = 1$, then the object is simply assigned to the class of that single nearest neighbor.

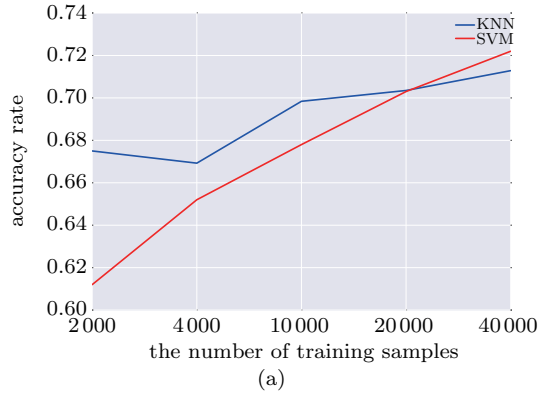

Figure 8 The test result of SVM. (a) Accuracy rate; (b) recall rate.

We define the accuracy rate and recall rate as $accuracy = n_{\text{correct}}/n_{\text{all}}$, $recall = n1_{\text{correct}}/n1_{\text{all}}$, where n_{all} is the number of all testing samples while n_{correct} is the number of all the correctly classified testing samples, i.e. the prediction of the interference indicator is correct. $n1_{\text{all}}$ is the number of all positive testing samples which means the number of all BSs suffering ADI interference. $n1_{\text{correct}}$ is the number of all correctly classified positive testing samples, i.e. the BSs suffering ADI interference are predicted correctly. The recall rate is more important for operators to improve network performance. This is because the greater the number of predicted interfered BSs, the more measures operators can take to avoid the impact of ADI.

The simulation results of the accuracy rate and recall rate are shown in Fig. 8 (a) and (b), respectively. Furthermore, because the SVM classifier is a machine learning algorithm, the accuracy rate and recall rate are approximately linearly increased when the number of training samples is increased. In Fig. 8(a), when the number of training samples is larger than 18 000, the accuracy rate of the SVM-classifier is better than that of KNN algorithm. In Fig. 8(b), when the number of training samples is larger than 14 000, the recall rate of the SVM-classifier is better than that of the KNN algorithm. When the number of training samples are 40 000, the accuracy rate and recall rate are 0.72 and 0.76, respectively. We can therefore conclude that better performance will be obtained when more samples are used to train the machine.

6 Implement a distributed linear SVM via ADMM

6.1 The forming of ADMM

Despite the result is not bad, in practice the network-side data is managed by prefecture-level city. To gather data is inconvenient and would require a large amount of time. Sometimes it is difficult because BSs may be produced by different equipment manufacturers.

To overcome these difficulties, we use a framework named ADMM, proposed in Ref. [19], to implement a distributed SVM. Moreover, ADMM introduces additional variables to regularize the difference among the models solved by the distributed machines.

The basic form of the ADMM problem is

$$\begin{aligned} \min_{\boldsymbol{x},\boldsymbol{z}} \quad & f(\boldsymbol{x}) + g(\boldsymbol{z}), \\ \text{s.t.} \quad & \boldsymbol{A}\boldsymbol{x} + \boldsymbol{B}\boldsymbol{z} = \boldsymbol{c}, \end{aligned} \tag{9}$$

where $f(x)$ and $g(z)$ are convex. The Augmented Lagrangian function is

$$L_\rho(x,z,y) = f(x) + g(z) + y^{\mathrm{T}}(Ax+Bz-c) + \frac{\rho}{2}\|Ax+Bz-c\|_2^2. \quad (10)$$

Recall formula (7), we now build up a z and rewrite Eq. (7) as the form of Eq. (9). To make the problem comfortable to decomposition, we let $\{B_1,\cdots,B_m\}$ be a partition of all data indices $\{1,\cdots,l\}$. By using ADMM framework, the equivalent problem is

$$\min_{\boldsymbol{\omega}_1,\cdots,\boldsymbol{\omega}_m,\boldsymbol{z}} \frac{1}{2}\|\boldsymbol{z}\|_2^2 + C\sum_{j=1}^{m}\sum_{i\in B_j}\max(1-y_i\boldsymbol{\omega}_j^{\mathrm{T}}\boldsymbol{x}_i,0)^2 + \frac{\rho}{2}\sum_{j=1}^{m}\|\boldsymbol{\omega}_j-\boldsymbol{z}\|_2^2, \quad \text{s.t. } \boldsymbol{\omega}_j-\boldsymbol{z}=0,\ j=1,\cdots,m. \quad (11)$$

Let us denote $\omega = \{\omega_1,\cdots,\omega_m\}$ and $\lambda = \{\lambda_1,\cdots,\lambda_m\}$. The Lagrangian of Eq. (11) is

$$L(\omega,\boldsymbol{z},\lambda) = \frac{1}{2}\|z\|_2^2 + C\sum_{j=1}^{m}\sum_{i\in B_j}\max(1-y_i\boldsymbol{\omega}_j^{\mathrm{T}}\boldsymbol{x}_i,0)^2 + \sum_{j=1}^{m}\left(\frac{\rho}{2}\|\boldsymbol{\omega}_j-\boldsymbol{z}\|_2^2+\lambda_j^{\mathrm{T}}(\boldsymbol{\omega}_j-\boldsymbol{z})\right), \quad (12)$$

where λ are the dual variables. ADMM consists of the following iterations:

$$\omega^{k+1} = \arg\min_{\omega} L\left(\boldsymbol{\omega},\boldsymbol{z}^{\boldsymbol{k}},\lambda^k\right), \quad (13)$$

$$\boldsymbol{z}^{k+1} = \arg\min_{\boldsymbol{z}} L\left(\boldsymbol{\omega}^{\boldsymbol{k+1}},\boldsymbol{z},\lambda^k\right), \quad (14)$$

$$\lambda_j^{k+1} = \lambda_j^k + \rho\left(\boldsymbol{\omega}_j^{k+1}-\boldsymbol{z}^{k+1}\right),\ j=1,\cdots,m. \quad (15)$$

L is separable in $\boldsymbol{\omega}_j$, so we can solve Eq. (13) in parallel as

$$\boldsymbol{\omega}_j^{k+1} = \arg\min_{\boldsymbol{\omega}'} \quad C\sum_{i\in B_j}\max\left(1-y_i\boldsymbol{\omega}'^{\mathrm{T}}\boldsymbol{x}_i,0\right)^2 + \frac{\rho}{2}\|\boldsymbol{\omega}'-\boldsymbol{z}\|_2^2+\lambda_j^{\mathrm{T}}(\boldsymbol{\omega}'-\boldsymbol{z}). \quad (16)$$

Also, $\boldsymbol{z}^{k+1}$ has a closed form solution

$$\boldsymbol{z}^{k+1} = \frac{\rho\sum_{j=1}^{m}\boldsymbol{\omega}_j^{k+1}+\sum_{j=1}^{m}\lambda_j^k}{m\rho+1}. \quad (17)$$

Letting $\boldsymbol{\mu}_j = \frac{\lambda_j}{\rho}$, we now have the ADMM iterations as

$$\boldsymbol{\omega}_j^{k+1} = \arg\min_{\boldsymbol{\omega}} C\sum_{i\in B_j}\max\left(1-y_i\boldsymbol{\omega}^{\mathrm{T}}\boldsymbol{x}_i,0\right)^2 + \frac{\rho}{2}\|\boldsymbol{\omega}-\boldsymbol{z}^k+\boldsymbol{u}_j^k\|_2^2, \quad (18)$$

$$\boldsymbol{z}^{k+1} = \frac{\sum_{j=1}^{m}\left(\boldsymbol{\omega}_j^{k+1}+\boldsymbol{u}_j^k\right)}{m+1/\rho}, \quad (19)$$

$$\boldsymbol{u}_j^{k+1} = \boldsymbol{u}_j^k + \boldsymbol{\omega}_j^{k+1} - \boldsymbol{z}^{k+1}. \quad (20)$$

Here, each machine j solves the subproblem (19) in parallel, which is only associated with data $\boldsymbol{X}_{B_j} = \{\boldsymbol{x}_i : i\in B_j\}$. Machine j also loads the data $\boldsymbol{X}_{B_j}$ from the disk only once and stores them in the memory in the ADMM iterations. Each machine only needs to communicate $\boldsymbol{w}_j$ and $\boldsymbol{u}_j$ without passing the data.

6.2 The prediction result of ADMM-SVM

In this simulation, the parameters are set the same as in section 5 with the difference that the training set was divided into four parallel subsets.

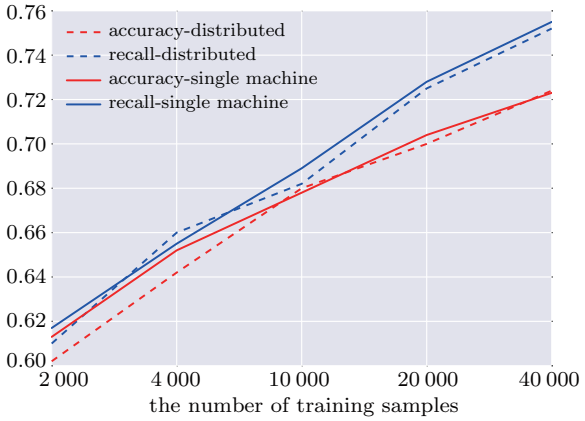

Figure 9 ADMM-SVM vs. single-machine SVM

The simulation result is shown in Fig. 9. We can find that both the accuracy rate and recall rate of ADMM-SVM are approximate to that of SVM. It means when operators want to improve the network performance, they can implement SVM-classifier in different cities/regions in parallel by exchanging only

limited amount of parameters. This is more practical to perform an overall SVM-classifier of the whole network.

7 Conclusion

In this paper, the ADI in large-scale TD-LTE networks was analyzed. Unlike the traditional atmospheric duct detection technology in meteorology, we started from the real network-side data provided by China Mobile. We performed a map-based visualization of interference data, and obtained the interference map of Jiangsu, China. We then analyzed the interference characteristics according to the interference map, correlation coefficient calculation and sector angles distribution.

The data analysis results verify the atmospheric duct phenomenon, and enable us to arrive at some interesting conclusions about the ADI characteristics:

- ADI has a time varying characteristic, probably occurring from midnight to morning.

- ADI has the feature of territoriality, and the rural regions have higher probability of suffering from ADI.

- ADI has a directional characteristic and the property of reciprocity.

- If the correlation coefficient of the interference data in two regions is closer to 1, the corresponding two regions have high probability to be pair of ADI objects.

In addition, we proposed an SVM-classifier based spacial prediction method of ADI, by machine learning over the combination of real network-side big data and real meteorological data. The simulation results show that the accuracy rate and recall rate approximately increase linearly when the number of training samples increases. When the number of training samples is 40 000, the accuracy rate can reach 72%, which outperforms the conventional KNN algorithm. Furthermore, a distributed algorithm of the ADMM-SVM prediction scheme is proposed and confirmed to exhibit the same performance as SVM. It enables operators to predict the ADI in a distributed manner without huge data exchange; it only communicates a small number of parameters, thus making it more practical to implement.

This paper is a starting point of ADI study. There remain many issues to be addressed in our future work. The first has to do with the statistical characteristic and modeling of ADI. The second is how to locate the exact interference source of ADI. The current data from China Mobile is rough from the perspective of the sector angles information, i.e., only three directions. A more detailed angle information, which may be obtained through field measurements, is required for ADI source location identification. The third is how to predict the occurrence of ADI in the time domain. So far, because of the lack of meteorological data with altitude, our method does not obtain a good result in predicting ADI in the time domain. More detailed meteorological data is therefore a key factor in ADI time varying prediction.

References

[1] B. R. Bean , E. J. Dutton. Radio meteorology [M]. New York: Dover Publications, 1966.

[2] S. S. Mentes, Z. Kaymaz. Investigation of surface duct conditions over Istanbul, Turkey [J]. Journal of applied meteorology and climatology, 2007, 46(3): 318-337.

[3] K. D. Anderson. Radar detection of low-altitude targets in a maritime environment [J]. IEEE transactions on antennas and propagation, 1995, 43(6): 609-613.

[4] P. Gerstoft, L. T. Rogers, W. S. Hodgkiss, et al. Refractivity-from-clutter using global environmental parameters [C]//IEEE 2001 International Geoscience and Remote Sensing Symposium, Sydney, Australia, 2001, 6: 2746-2748.

[5] H. Oraizi, S. Hosseinzadeh. The effect of atmospheric duct on modern OFDM-based digital broadcasting systems [C]//The 33rd European Microwave Conference, Munich, Germany, 2003: 747-750.

[6] X. H. Li, Z. S. He, J. X. He, et al. Design of an ocean atmospheric duct signal processor [C]//International Symposium on Intelligent Signal Processing and Communication Systems (ISPACS), Chengdu, China, 2010: 1-4.

[7] 3GPP. Technical Specification Group Radio Access Network; Evolved Universal Terrestrial Radio Access (E-UTRA); Physical Channels and Modulations (Release 8). 3GPP TS 36.213 version 8.8.0 [S]. 3rd Generation Partnership Project, 2009: 11

[8] J. Hofmann, R. van der Pol V, G. Sébire, et al. 3GPP Release 8 [C]//GSM/EDGE: Evolution and Per-

formance, Wiley, 2011: 63-99.
[9] Laster J D, Reed J H. Interference rejection in digital wireless communications [J]. IEEE signal processing magazine, 1997, 14(3): 37-62.
[10] W. J. Lu, Q. Fan, Z. X. Li, et al. Power control based time-domain inter-cell interference coordination scheme in DSCNs [C]//IEEE International Conference on Communications (ICC), Kuala Lumpur, Malaysia, 2016: 1-6.
[11] A. Jeremic, T. A. Thomas, A. Nehorai. OFDM channel estimation in the presence of interference [J]. IEEE transactions on signal processing, 2004, 52(12): 3429-3439.
[12] W. X. Xu, S. Sezginer. Co-channel interference cancellation in reuse-1 deployments of WiMAX system [C]//IEEE Wireless Communications and Networking Conference (WCNC), Paris, France, 2012: 342-346.
[13] E. C. Kim, J. Y. Kim, H. J. Choi, et al. Co-channel interference cancellation based on SIC with optimal ordering for cooperative communication systems [C]//Digest of Technical Papers International Conference on Consumer Electronics (ICCE), Las Vegas, USA, 2010: 277-278.
[14] G. Mao, B. D. O. Anderson, B. Fidan. Path loss exponent estimation for wireless sensor network localization [J]. Computer Networks, 2007, 51(10): 2467-2483.
[15] P. A. Burrough, R. A. McDonnell, R. McDonnell, et al. Principles of geographical information systems [M]. Oxford: Oxford University Press, 2015.
[16] M. L. Stein. Interpolation of spatial data: some theory for kriging [M]. New York: Springer Science+Business Media New York, 2012.
[17] J. C. Platt. Sequential minimal optimization: a fast algorithm for training support vector machines [C]//Advances in Kernel Methods-support Vector Learning, 1998: 212-223.
[18] D. T. Larose. k-nearest neighbor algorithm [C]//Discovering knowledge in data: an introduction to data mining, Wiley, 2005: 90-106.
[19] S. Boyd, N. Parikh, E. Chu, et al. Distributed optimization and statistical learning via the alternating direction method of multipliers [J]. Foundations and trends in machine learning, 2011, 3(1): 1-122.

About the authors

Ting Zhou was borned in Jun. 1982, Guangdong province. She received the B.S. degree and M.S. degree from the Department of Electronic Engineering of Tsinghua University in 2004 and 2006, and PhD. degree from Shanghai Institute of Microsystem and Information Technology (SIMIT) of Chinese Academy of Sciences (CAS) in 2011. From 2011 to 2013, she worked at Shanghai Research Center for Wireless Communication as a research assistant in SIMIT. From January 2014 to the present, she is an associate professor at Shanghai Research Center for Wireless Communication in SIMIT. She is currently mainly focuses on resource management and intelligent networking of heterogeneous wireless networks. She won 2015 first prize of China Institute of Communication Technical Innovation Award and 2015 second prize of Shanghai Science and Technology Progress Award. She has been authored or co-authored over 20 papers published in journals and conferences, and 44 granted and pending patents. (Email: ting.zhou@mail.sim.ac.cn)

Tianyu Sun received B.S. degree in College of Telecommunications & Information Engineering, Nanjing University of Posts and Telecommunications. He is now a postgraduate student in Shanghai Research Center for Wireless Communication. He is currently mainly research on data mining in wireless communication.

Honglin Hu [corresponding author] received the Ph.D. degree in communications and information systems from the University of Science and Technology of China, Hefei, China, in 2004. He was with Future Radio, Siemens AG Communications, Munich, Germany, until 2005. In 2006, he joined the Shanghai Institute of Microsystem and Information Technology, Chinese Academy of Sciences, Shanghai, China, where he has served as a full professor (since 2009). He also serves as an adjunct professor with ShanghaiTech University, Shanghai, and the vice director of the Shanghai Research Center for Wireless Communications (WiCO), Shanghai. He was the vice chair of the IEEE Shanghai Section (2008-2012) and a member of IEEE WTC/ComSoc. In addition, he served as a Technical Program Committee Member and the co-chair for many international conferences, such as IEEE International Conference on Communications from 2006 to 2014, and the IEEE Global Communications Conference from 2007 to 2014. He serves as an associate editor of four international journals. He is the leading guest editor of the IEEE Wireless Communications special issue on mobile converged networks. (Email: honglin.hu@mail.sari.ac.cn)

Hui Xu received the B.Eng. and M.Eng. degrees in Communication Engineering from Shanghai Jiao Tong University, Shanghai, China, in 2004 and 2008, respectively. Hui Xu is currently a senior engineer with Shanghai Institute of Microsystem and Information Technology (SIMIT), Chinese Academy of Sciences,

serving as the department head of CAS Key Laboratory of Wireless Sensor Network and Communication, and the department head of Shanghai Research Center for Wireless Communications (WiCO). Prior to that, he has served the Department of Global Telecom Solutions Sector at MOTOROLA (China) co., LTD, as a R&D Senior Engineer; and the Department of Production Quality at Shanghai Datang Telcom, China, as a R&D Engineer. His research interests include wireless communication networks, software defined wireless networks, 5G mobile systems, intelligent transport systems, wireless testbed development and practical experiments. (Email: hui.xu@wico.sh)

Yang Yang received the B.Eng. and M.Eng. degrees in radio engineering from Southeast University, Nanjing, China, in 1996 and 1999, respectively; and the Ph.D. degree in information engineering from The Chinese University of Hong Kong in 2002. Dr. Yang Yang is currently a professor with Shanghai Institute of Microsystem and Information Technology (SIMIT), Chinese Academy of Sciences, serving as the director of CAS Key Laboratory of Wireless Sensor Network and Communication, and the director of Shanghai Research Center for Wireless Communications (WiCO). He is also an adjunct professor with the School of Information Science and Technology, ShanghaiTech University. Prior to that, he has served the Department of Electronic and Electrical Engineering at University College London (UCL), United Kingdom, as a senior lecturer; the Department of Electronic and Computer Engineering at Brunel University, United Kingdom, as a lecturer; and the Department of Information Engineering at The Chinese University of Hong Kong as an assistant professor. His research interests include wireless ad hoc and sensor networks, software defined wireless networks, 5G mobile systems, intelligent transport systems, wireless testbed development and practical experiments. Dr. Yang Yang has co-edited a book on heterogeneous cellular networks (2013, Cambridge University Press) and co-authored more than 100 technical papers. He has been serving in the organization teams of about 50 international conferences, e.g. a co-chair of Ad-hoc and Sensor Networking Symposium at IEEE ICC'15, a co-chair of Communication and Information System Security Symposium at IEEE Globecom'15. (Email: yang.yang@wico.sh)

Ilkka Harjula works as a senior scientist at VTT Technical Research Centre of Finland. He received his M.Sc. degree in telecommunications from the University of Oulu in 2002 and Licentiate of Technology in 2008, and is currently working towards a Ph.D., focusing on energy and spectrum efficient technologies for 5G systems. Ilkka has contributed to numerous national and international R&D projects studying the communication concepts associated with 5G systems as well as the functionalities of currently dominating commercial technologies, such as LTE, WiMAX, and WLAN. He has also authored or co-authored over 20 journal articles, conference papers and book chapters covering these topics. He has several pending patent applications related to 5G technologies. (Email: Ilkka.Harjula@vtt.fi)

Yevgeni Koucheryavy is a full professor at the Tampere University of Technology (TUT), Finland. Yevgeni holds Ph.D. degree (2004) from the TUT. He has worked in a number of research and development projects within different frameworks, e.g., FP7, H2020, and companies including Nokia, Ericsson, Intel and others. Within last 5 years (2012 C 2016) he managed to attract over 5 mln Euros as a research funding from the external sources. He is an expert in the Skolkovo Foundation(Russia) and acts as an external reviewer for state funding agencies of several European countries. He has authored or co-authored over 200 papers in the field of advanced wired and wireless networking and communications. He holds one US patent and 3 pending. His current research interests include various aspects in heterogeneous wireless communication networks and systems 5G and beyond, network and services performance evaluation, the Internet of Things and its standardization, nanocommunications. He is an associate technical editor of IEEE Communications Magazine, editor of IEEE Communications Surveys and Tutorials and editor of IEEE Communication Society Technology News. He is a senior IEEE member. Yevgeni is a co-founder and chairman of the Board of Finnish company YL-verkot Oy offering leading innovative technological solutions in 5G and Industrial IIoT domains. (Email: evgeni.kucheryavy@tut.fi)